Eur J Trauma Emerg Surg (2018) 44:351–368
DOI 10.1007/s00068-017-0838-y

REVIEW ARTICLE

Pediatric head trauma: an extensive review on imaging requisites and unique imaging findings

F. C. Sarioglu[1] · H. Sahin[1] · Y. Pekcevik[1] · O. Sarioglu[2] · O. Oztekin[1]

Received: 2 March 2017 / Accepted: 12 September 2017 / Published online: 15 September 2017

Abstract The effects of trauma in children are different due to association with some anatomical and physiological differences compared with adults. The role of neuroimaging gains importance in early detection of traumatic brain injuries and prevention of secondary post-traumatic complications. Many algorithms are described for children with head trauma to decide the necessity of a computed tomography scan. The aims of this article are to describe differences of these algorithms, the mechanism of traumatic brain injury with radiological imaging findings in the pediatric population, and explain complications of undiagnosed traumatic brain lesions.

Keywords Pediatrics · Craniocerebral trauma · CT · MRI · Brain injuries

Introduction

Traumatic brain injury (TBI) is a leading cause of death and disability. In many countries, vehicle accidents and falling are the most common causes of head trauma in the pediatric population. The effects of trauma in children are different compared with adults. The main reasons for this difference are that the skull is thinner and more flexible, the head-to-body ratio is larger, the protective muscles are less, and the cervical ligaments and joints are more flexible in children when compared with adults [2]. Furthermore, cerebral blood flow (CBF) is higher during brain development and declines with maturation, and a phase of maximal synaptogenesis is closely related to this increased CBF [2]. For that reason, TBI may cause an arrest in the neurological development process in the follow-up period after trauma, and hence, physical, cognitive, and behavioral system disabilities may occur.

In this article, we provide a comprehensive review for pediatric TBI with an emphasis on imaging findings. Current algorithms in pediatric head trauma are also reviewed, to guide that clinicians about the appropriate time of computed tomography (CT) scanning should be performed. In addition, after reviewing this article, the reader will be able to understand acute and chronic head injury types with mechanisms of injury. There have been numerous studies in the literature about either imaging findings of the pediatric TBI [2, 3] or CT algorithms in children with head trauma [4–6]. However, to our knowledge, there has been no reviews discussing the pediatric head trauma comprehensively in consideration both those subjects.

Which algorithms can be used in children with head trauma for decision of CT scanning?

The major problem about management of TBI is whether the cranial CT scanning should perform. Numerous studies have been published regarding which algorithms should be used in children with head trauma for a decision of CT scanning. The Pediatric Emergency Care and Applied Research Network (PECARN), the children's head injury algorithm for the prediction of important clinical events (CHALICE),

This review article has been published as an electronic poster in ECR 2016 [1].

✉ F. C. Sarioglu
drcerenunal@gmail.com

[1] Department of Radiology, Tepecik Training and Research Hospital, 35110 Yenisehir, Izmir, Turkey

[2] Department of Radiology, Dokuz Eylul University Faculty of Medicine, Izmir, Turkey

and Canadian Assessment of Tomography for Childhood Head injury (CATCH) are three of the most well-known studies of clinical decision rules for head trauma in pediatric groups [4–6].

There have been several differences among three studies. The main difference between those studies is that the CATCH and CHALICE determine the group of children who require CT; on the other hand, PECARN determines who do not. In addition, other differences are population, outcomes, age limitations, and inclusion and exclusion criteria. The purpose of the PECARN clinical decision rule is to determine indications of CT scanning for children with very low risk of TBI. The inclusion criteria of the PECARN algorithm are age less than 18 years, Glasgow Coma Scale score (GCSS) of 14–15 and admission to the hospital within 24 h of head trauma. The exclusion criteria of this algorithm are children with trivial mechanism of injury defined by ground-level fall or running into stationary objects, and no signs or symptoms of head trauma other than scalp abrasions and lacerations, penetrating trauma, known brain tumors, pre-existing neurological disorder, complicated assessment, neuroimaging at an outside hospital before transfer, ventricular shunt, bleeding disorder, and GCSS less than 14. The study suggests two algorithms based on the age of the patients: children younger 2 years, children 2 years and older [4]. Table 1 summarizes the PECARN clinical decision rule. The aims of the CHALICE clinical decision rule are to identify children who are less than 16 years with head injuries of any severity that require a CT scan of the head and to allow the remaining patients to be discharged with no investigation [5]. There are no exclusion criteria in this rule. The CHALICE rule is summarized in Table 2. The aim of the CATCH rule is to develop clinical decision rules for the use of CT in children with minor head injuries. This study differs from PECARN rule in that it does not distinguish the algorithms according to the age of the patients. Minor head injury is defined as blunt trauma to the head resulting in witnessed loss of consciousness, definite amnesia, witnessed disorientation, persistent vomiting (two or more distinct episodes of vomiting 15 min apart) or persistent irritability in the emergency department (for children under 2 years of age), initial score on the GCSS in the emergency department of at least 13, as determined by the treating physician, and injury within the past 24 h. A patient should meet all of these criteria to use the CATCH rule. In addition, in this study, there are two risk groups in children with minor head injuries: high risk (need for neurosurgical intervention) and medium risk (brain injury on CT scan). According to the CATCH rule, CT scanning is required only for children with minor head injury and any one of the high-risk or medium-risk findings. This study suggested that high-risk patients that require CT scanning are those with failure to reach GCSS of 15 within 2 h, suspicion of open or depressed skull fracture, worsening headache, and irritability on examination; whereas large scalp hematoma, signs of skull base fracture, and dangerous injury mechanism were identified as medium-risk factors. Patients should be excluded if they have obvious penetrating skull injury or obvious depressed fracture, acute focal neurologic deficit, chronic generalized developmental delay, or head injury secondary to suspected child abuse [6].

A comparison among those algorithms is not possible because of the differences in their criteria. However, two prospective cohort studies [7, 8] have indicated that PECARN rule is more sensitive than other studies.

Imaging modalities

The role of neuroimaging has become important in the early detection of traumatic brain injuries and prevention of secondary post-traumatic complications. CT is commonly used initially for the rapid detection of TBI. The advantage of CT is the demonstration of ventricular size and configuration, bone injuries, and acute hemorrhage [9]. Although MRI is more sensitive in demonstrating hemorrhagic lesions, CT scanning is more widely used, since it is quicker and cheaper than MRI. However, children are more sensitive to stochastic effects of ionizing radiation than adults and have potential cancer risks, especially leukemia and brain tumors [10]. In addition, there are some limitations of CT scanning in traumatic patients, such as small and nonhemorrhagic lesions, vascular injury, cerebral edema, hypoxic–ischemic brain injury (HIBI), or patients with severe anemia [3].

MRI is sensitive for detecting and characterizing subacute and chronic brain injuries. MRI is generally considered to be superior to CT after 48–72 h from injury. MRI is better than CT in detecting subacute–chronic hematomas with changing blood products [11–13]. In case of a discrepancy between CT findings and clinical status, MRI should be performed. It is also superior to CT in establishing nonhemorrhagic primary lesions, traumatic posterior fossa lesions, and the secondary effects of trauma [3]. Diffusion-weighted imaging (DWI) is sensitive in detecting HIBI and diffuse axonal injury (DAI) which are subtle on T2-weighted images. T2*-weighted gradient echo (T2*-GRE) and susceptibility-weighted imaging (SWI) sequences are sensitive to paramagnetic blood products. SWI differs from T2*-GRE in that SWI is based on a long echo time, high-resolution, flow compensation, and filtered phase information in each voxel [14]. SWI is very sensitive in detecting small areas of hemorrhages as well as in differentiating calcium and other diamagnetic substances from blood (paramagnetic) which can be in similar density in CT [14–16]. Cerebral catheter angiography, CT angiography (CTA), and MR angiography (MRA) also have roles in the diagnosis and management

Table 1 Pediatric Emergency Care and Applied Research Network: the PECARN rule (Reprinted, with permission, from reference [4])

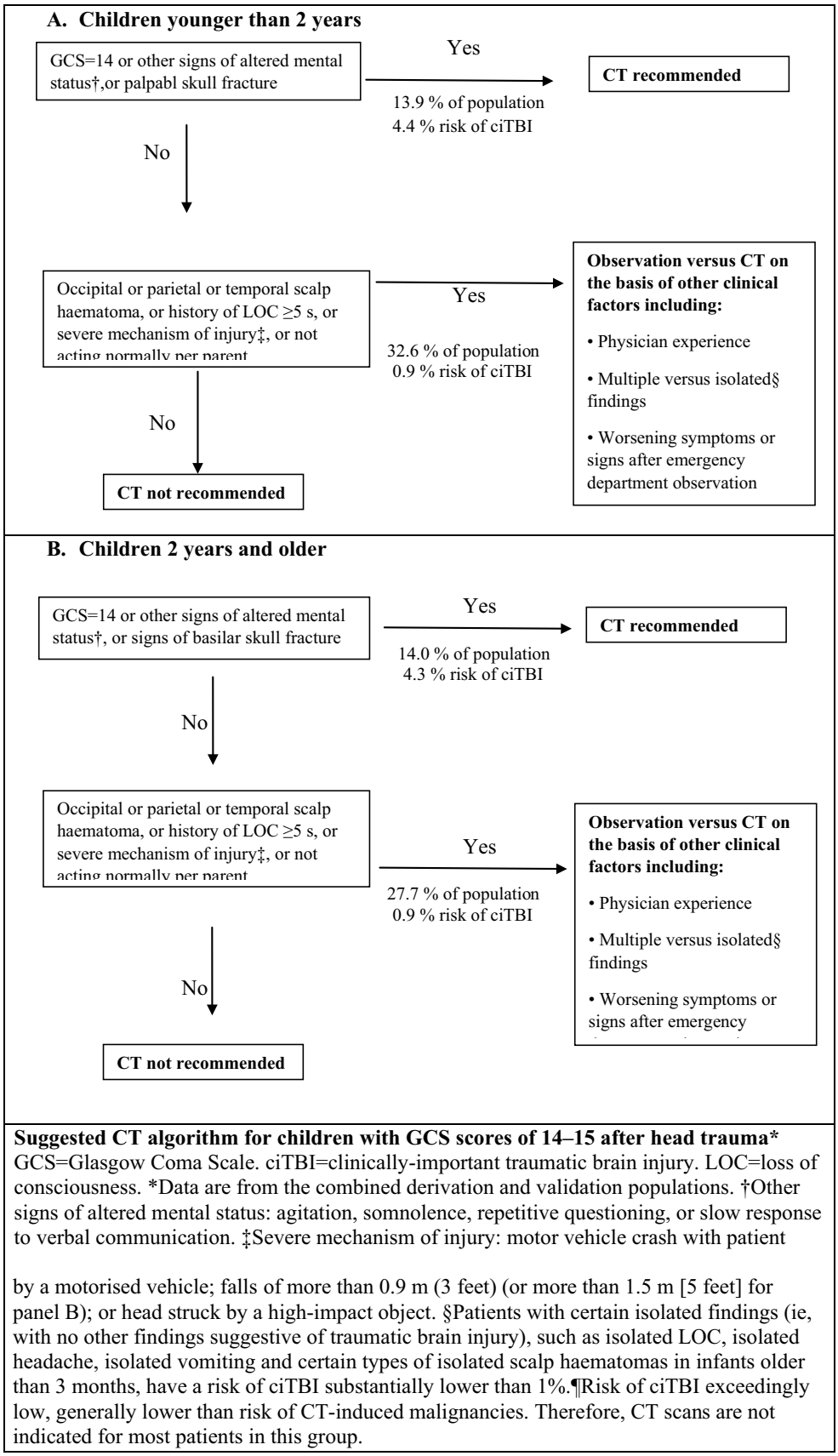

Suggested CT algorithm for children with GCS scores of 14–15 after head trauma*
GCS=Glasgow Coma Scale. ciTBI=clinically-important traumatic brain injury. LOC=loss of consciousness. *Data are from the combined derivation and validation populations. †Other signs of altered mental status: agitation, somnolence, repetitive questioning, or slow response to verbal communication. ‡Severe mechanism of injury: motor vehicle crash with patient

by a motorised vehicle; falls of more than 0.9 m (3 feet) (or more than 1.5 m [5 feet] for panel B); or head struck by a high-impact object. §Patients with certain isolated findings (ie, with no other findings suggestive of traumatic brain injury), such as isolated LOC, isolated headache, isolated vomiting and certain types of isolated scalp haematomas in infants older than 3 months, have a risk of ciTBI substantially lower than 1%.¶Risk of ciTBI exceedingly low, generally lower than risk of CT-induced malignancies. Therefore, CT scans are not indicated for most patients in this group.

Table 2 Children's head injury algorithm for the prediction of important clinical events rule: the CHALICE rule (Reprinted, with permission, from reference [5])

A computed tomography scan is required if any of the following criteria are present
History
Witnessed loss of consciousness of > 5 min duration
History of amnesia (either antegrade or retrograde) of > 5 min duration
Abnormal drowsiness (defined as drowsiness in excess of that expected by the examining doctor)
≥ 3 vomits after head injury (a vomit is defined as a single discrete episode of vomiting)
Suspicion of non-accidental injury (NAI, defined as any suspicion of NAI by the examining doctor)
Seizure after head injury in a patient who has no history of epilepsy
Examination
Glasgow Coma Score (GCS) < 14, or GCS < 15 if < 1 year
Suspicion of penetrating or depressed skull injury or tense fontanelle
Signs of a basal skull fracture (defined as evidence of blood or cerebrospinal fluid from ear or nose, panda eyes, Battles sign, haemotympanum, facial crepitus or serious facial injury)
Positive focal neurology (defined as any focal neurology, including motor, sensory, coordination or reflex abnormality)
Presence of bruise, swelling or laceration > 5 cm if < 1 year
Mechanism
High-speed road traffic accident either as pedestrian, cyclist or occupant (defined as accident with speed 40 m/h)
Fall of > 3 m in height
High-speed injury from a projectile or an object
If none of the above variables are present, the patient is at low risk of intracranial pathology

of traumatic vascular injuries [17]. Radiological images should be evaluated in conjunction with the associated clinical symptoms such as fixed lateralizing or focal neurologic deficits [18]. However, some patients with vascular injury may present without symptoms [19].

Advanced neuroimaging techniques can be used to identify TBI and predict the outcome. Some of these techniques are diffusion tensor imaging (DTI), blood-oxygen-level dependent (BOLD) functional MRI (fMRI), MR spectroscopy (MRS), and perfusion imaging [20]. DTI eliminates the directional effects of anisotropic diffusion and provides pure diffusion information. Tractography is the method displaying three-dimensional images of white matter tracts or similar tubular structures using the tensor data. It is useful in assessing the white matter fiber pathways between brain regions. In addition, it is sensitive to microstructural changes, particularly in white matter, whereas CT and conventional MRI reveal only macroscopic changes in the brain [21]. The BOLD monitoring is an fMRI technique that is based on the change of diamagnetic oxyhemoglobin to paramagnetic deoxyhemoglobin with brain activation [22–24]. Children's brains undergo many changes such as brain maturation, connectivity, and cortical organization in the first few years of life. The mapping of motor and cognitive functions for presurgical planning with fMRI is gaining an important role in children with head trauma. MRS, which is a method used in chemistry to identify and quantify metabolites in samples, provides a sensitive assessment of neurochemical alterations [20]. Commonly quantified brain metabolites are *N*-acetylaspartate (NAA), creatine (Cr), choline (Cho), and lactate. Metabolite levels vary with the severity of the injury and post-traumatic complications [20]. Indeed, the common result of several studies is that NAA levels and ratios associated with NAA levels (NAA/Cr and NAA / Cho) decrease after TBI [24, 25]. Another technique which may be used in the assessment of TBI is the perfusion imaging which demonstrates regional brain perfusion alterations due to TBI [26]. Brain perfusion in patients with TBI could be performed with different techniques, including Xenon clearance technique, xenon CT, single-photon-emission CT, positron-emission tomography, perfusion CT, and arterial spin labeling [26]. After TBI, the blood flow of the middle cerebral artery decreases resulting in cerebral hypoperfusion and associated cerebral ischemia. In addition, it is reported that normal or increased CBF may cause cerebral hyperemia and hemorrhage may occur [26]. Finally, poor outcome may occur.

Imaging findings of head trauma

Skull fractures

When compared with adults, skull fractures are less common in children, because bones are pliable during childhood. Distinguishing skull fractures from normal structures or variants is not always easy. Normal and accessory sutures, vascular grooves, wormian bones, and molding may imitate

skull fractures. Sutures are usually bilateral and identified by their typical zigzag course and sclerotic borders, but fractures have linear fissure with lack of sclerotic margin [27]. Vascular grooves have well-corticated margins, and they are not as sharp or lucent as linear skull fractures. In addition, swelling adjacent to soft tissue, pneumocephalus, and effusion in sinuses is important clues for fractures.

Skull fractures can be classified as linear, depressed, diastatic, ping pong, and growing skull fracture [3]. Linear fractures are the most common fractures, and bones do not displace in these fractures (Fig. 1). Depressed fractures involve fragments of bone that are depressed deeper than the inner table (Fig. 2). Diastatic fracture occurs along the suture lines, so normal suture lines are widened. Ping-pong fractures are depressed fractures similar to greenstick fracture of the long bones in children in which the fracture line appears concave (Fig. 3). Another interesting term is the growing skull fracture, or "leptomeningeal cyst." It is a rare complication of skull fractures in children and arises from a skull fracture related to dural tear and repeated pulsations of cerebral spinal fluid (CSF) [28]. Eventually, the calvarial margin adjacent to the fracture expands, giving the sense of "growing" (Fig. 4). The differential diagnosis of a leptomeningeal cyst includes congenital (cephalocele) or iatrogenic (pseudomeningocele) cystic lesions (Fig. 5). Besides, eosinophilic granuloma and infection should also be thought in the differential diagnosis [29, 30]. Skull base fractures are particular group of fractures which should be recognized owing to a probable injury of cranial nerves and vessels (Fig. 6). They are mainly located in the temporal bone or occipital condyle. Temporal skull base fractures are divided into three subtypes: longitudinal, transverse, and mixed. Longitudinal fractures involve the squamous part of the temporal bone and course parallel to the long axis of the petrous bone. These types of fracture may cause a conductive hearing loss due to ossicular injury, tympanic membrane rupture, hemotympanum, and less commonly, facial nerve injury [31]. Facial paralysis is a rare delayed complication of longitudinal fracture. There are two mechanisms of delayed facial paralysis; entrapment of a nerve within fibrous tissue contiguous to fracture, which is more common and other is due to nerve edema within fallopian canal [31, 32]. Contrary

Fig. 2 A 2-year-old girl was presented after a road traffic accident. Axial NECT scan shows depressed fracture of right inferior frontal bone (arrow)

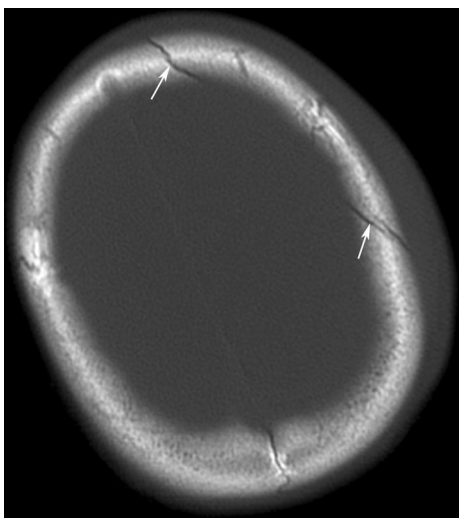

Fig. 1 A 7-year-old boy was presented after a road traffic accident. Axial non-contrast enhanced CT (NECT) scan shows nondisplaced fracture of left frontal bone (arrow) with soft tissue swelling

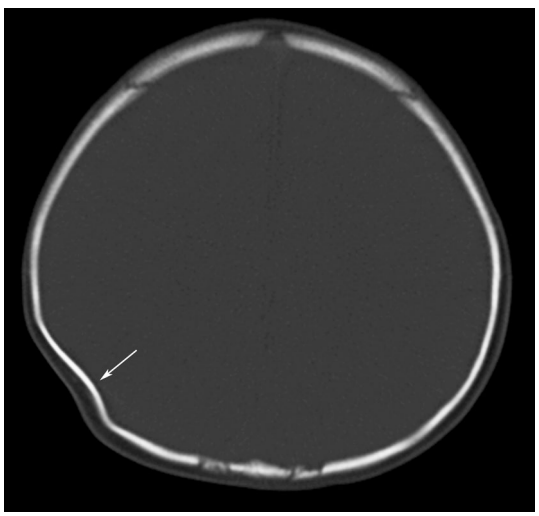

Fig. 3 A 6-month-old baby was presented after falling down from 2 m. Axial NECT scan shows ping-pong fracture in right parietal bone (arrow)

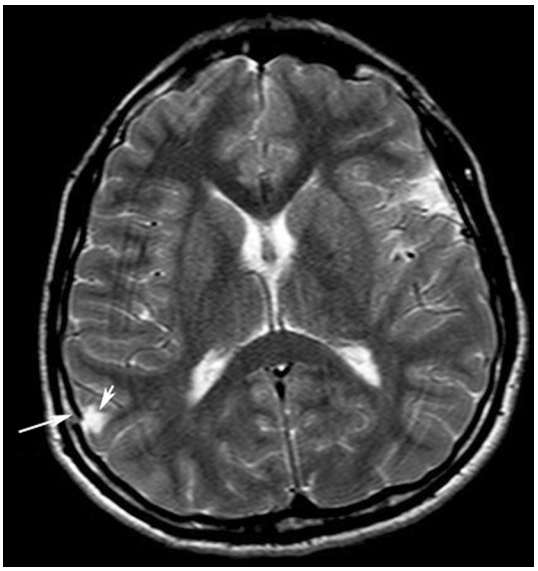

Fig. 4 An 8-year-old boy presented with a traffic accident and MRI was performed after 6 months from trauma. Axial T2-weighted image shows small leptomeningeal cyst which is seen hyperintense (short arrow) adjacent to fracture of internal tabula (long arrow)

to longitudinal fractures, transverse fracture lines are perpendicular to the long axis of the petrous bone. They are often associated with sensorineural hearing loss which may occur secondary to injury of labyrinthine structures or transection of the cochlear nerve. In addition, facial paralysis is more common in patients with a transverse fracture [31].

Although CT is the best modality for fracture assessment, fracture lines which are parallel to the section plane can easily be overlooked. Multiplanar reformatting in CT with three-dimensional bony reconstruction is important notably in those cases and may help not to miss those fractures (Fig. 7) [33, 34].

Epidural hemorrhage (EDH)

EDH occurs between the outer layer of the dura mater and the inner table of the calvarium. This kind of extra-axial hemorrhage is caused by injury of the middle meningeal artery, dural venous sinuses, and veins. The source of hemorrhage is usually arterial (85% for adults). However, the middle meningeal artery is not embedded in the calvarium in children; thus, arterial temporal EDH is rare [13, 35]. Tearing of a dural venous sinus results in a venous EDH along the transverse sinus, torcula, or superior sagittal sinus. EDH does not cross suture lines, whereas can extend across the falx cerebri and tentorium (Fig. 8). Acute EDH is seen as hyperdense, biconvex-shaped collection in the extra-axial region on CT. "*Swirl sign*" is described as a hypodense area in a hyperdense collection that indicates active bleeding (Fig. 9) [36]. Skull fracture is generally associated with

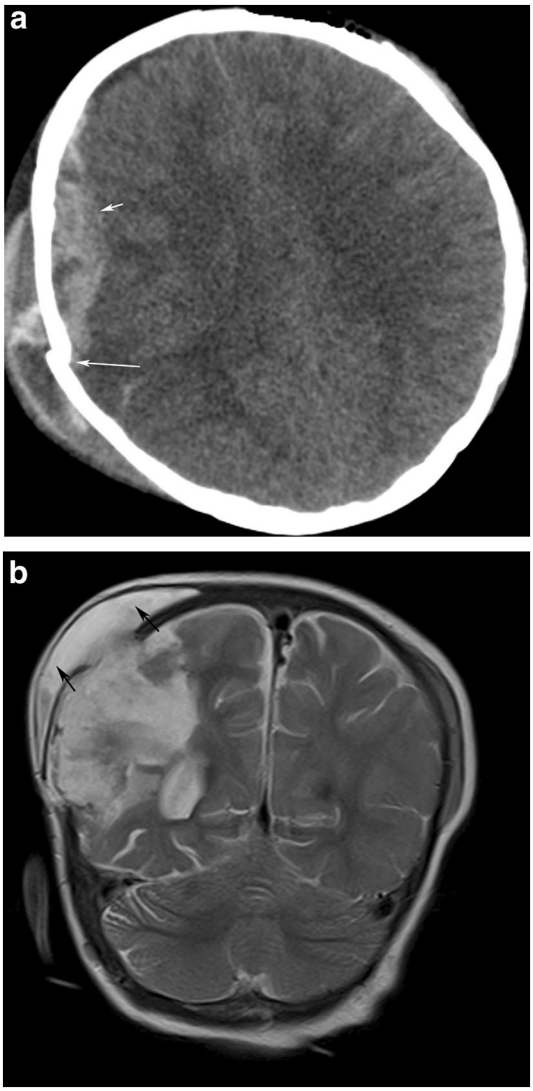

Fig. 5 A 9-month-old girl was presented after a road traffic accident. **a** Axial NECT scan shows EDH in right frontal lobe (short arrow) with depressed fracture (long arrow). **b** Coronal T2-weighted image performed after 4 weeks from craniectomy operation shows pseudomeningocele (black arrows)

EDH, although, in children, EDH can occur without a fracture. Notably, the posterior fossa EDH can mimic a dural venous thrombosis by compressing and displacing sinuses [35]. Diagnosis of dural venous sinus thrombosis should be considered if there is occipital bone fracture adjacent to the dural sinuses. The confirmation of the diagnosis relies on the demonstration of thrombus by neuroimaging techniques such as MR venography [37].

Subdural hemorrhage (SDH)

SDH is located between the dura and arachnoid mater. SDH, which is caused by the tearing of bridging veins, presents

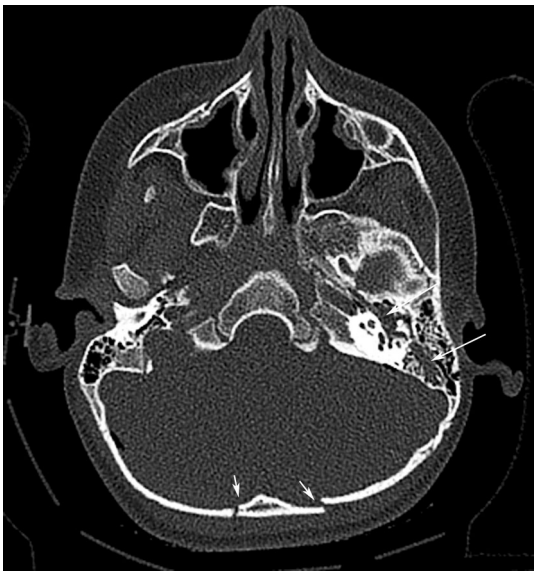

Fig. 6 A 2-year-old boy was presented after falling down from 2 m. Axial NECT scan shows bilateral occipital bone fractures (short arrows) and hemorrhagic opacification in left mastoid cells and middle ear cavity (long arrows). Temporal bone fracture is not shown

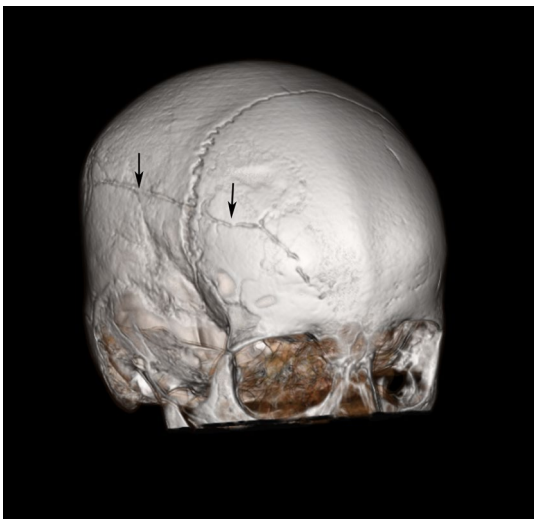

Fig. 7 A 6-year-old girl was presented after falling from 2 m. Non-displaced fracture of frontal and parietal bone is seen in CT 3D bony reconstruction (arrows). It was not seen in axial CT scan (not shown)

Fig. 8 A 11-year-old boy was presented after a road traffic accident. Axial CT scan shows EDH in frontal region, crossing the anterior falx (arrows)

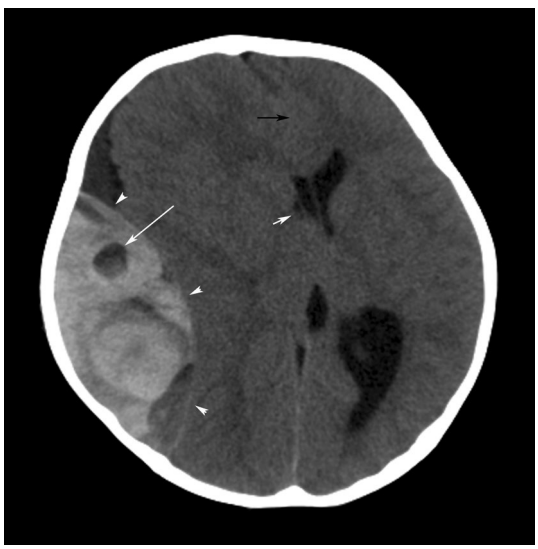

Fig. 9 A 19-month-old girl was presented after falling from 3 m. Axial NECT scan shows large temporal EDH which is biconvex in shape (arrowheads). The "*swirl sign*" (long white arrow) is seen suggesting active bleeding, accompanying midline shift (black arrow) and compressed right ventricle (short white arrow)

as a crescent-shaped collection in the extra-axial region (Fig. 10). SDH, contrary to EDH, may cross suture lines; however, it does not cross the midline owing to the falx cerebri. Large SDH may cause mass effect and herniations. Large mass effect may result in cerebral infarction due to compression of the anterior or posterior cerebral artery [38].

The appearance of hemorrhage may vary according to the age of blood products. MRI may be useful for age determination in this context [12, 13]. In addition, MRI is more sensitive than CT for determination of small SDH. However, the variation in MRI signal intensity may not always help to determine the age of the extra-axial hemorrhage due to the vascularized dura created by high oxygen tension in the subdural space. The time interval between the different stages of SDHs on CT and MRI is generally

Fig. 10 A 7-year-old boy was presented after a road traffic accident. On axial NECT scan, acute SDH is seen with a concave shape in right frontoparietal and temporal lobes (arrows)

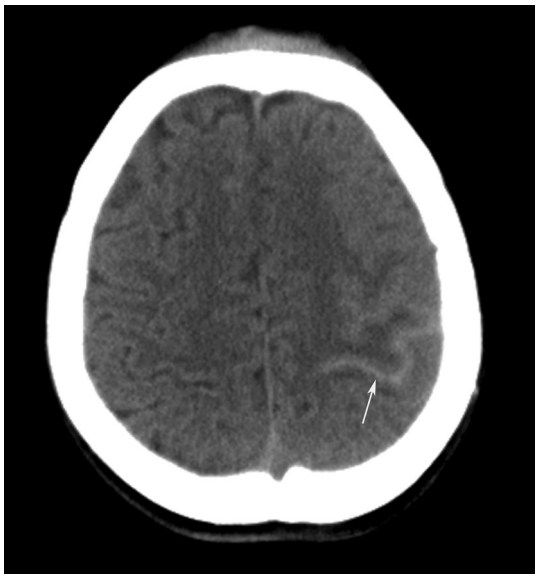

Fig. 11 A 12-year-old girl was presented after falling from 3 m. Axial NECT scan demonstrates SAH in left frontal and parietal sulci (arrow)

broad and overlaps. This is an important concept that can lead to serious incidents in case of medico-legal trials related to a non-accidental injury. Therefore, CT or MRI findings are not precise and reliable to determine the accurate date of SDHs [39].

Subarachnoid hemorrhage (SAH)

SAH occurs between the arachnoid and pia mater. SAH and intraventricular hemorrhage can be very subtle. The diagnosis is suspected when a hyperdense material is seen filling the subarachnoid spaces (i.e., the basal cisterns, sulci, and Sylvian fissure) on CT (Fig. 11). However, in MRI, T2 fluid-attenuated inversion recovery (FLAIR) sequence is the most useful sequence for acute SAH, which must be distinguished from other pathological and artifactual causes, such as meningitis, hyperoxygenation therapy, or CSF flow artifacts, that can cause high signal intensity in the sulci on FLAIR images [40, 41]. Sites of hyperintensity, especially in basal cisterns such as the interpeduncular, perimesencephalic, prepontine, and ambient cisterns, and clinical findings can facilitate the diagnosis of SAH. Retrograde flow of SAH may result in intraventricular hemorrhage (IVH) through the foramen of Luschka or Magendie. Blood–CSF level in occipital horns of lateral ventricle is a typical appearance of IVH [42]. SAH should be recognized immediately to prevent complications, such as hydrocephalus, infarction due to cerebral vasospasm, and cerebral herniation, which can lead to rapid progression to coma.

Diffuse axonal injury (DAI)

DAI, also known as "shearing injury," occurs in subcortical white matter, deep white matter, corpus callosum, and brain stem [43]. The typical mechanism of axonal damage is a rotational acceleration and deceleration movement of axons due to a traumatic event. According to the Adams grading system, DAI is divided into three grades, based on the location of injury in the cerebral hemispheres. Injury with predilection for the gray–white matter interface forms grade 1, the corpus callosum grade 2, and the brainstem grade 3 DAI [44]. In imaging, DAI is frequently characterized by punctate nonhemorrhagic or hemorrhagic lesions.

Imaging findings on CT are often normal initially. Punctate hemorrhagic lesions may appear as hyperdense foci on CT [45]. Although CT is the initial imaging method in trauma patients, DAI should be considered, and further evaluation with MRI should be performed in patients who clinically deteriorate. In MRI, the appearance of hemorrhagic DAI lesions varies widely due to the age of the hemorrhage. Nonhemorrhagic DAI lesions can be demonstrated at their characteristic locations with high signal intensity (SI) on T2-weighted images and low SI on T1-weighted images (Fig. 12). In addition, DWI can demonstrate both nonhemorrhagic and hemorrhagic DAI lesions that are not visualized with the conventional MR sequences [46].

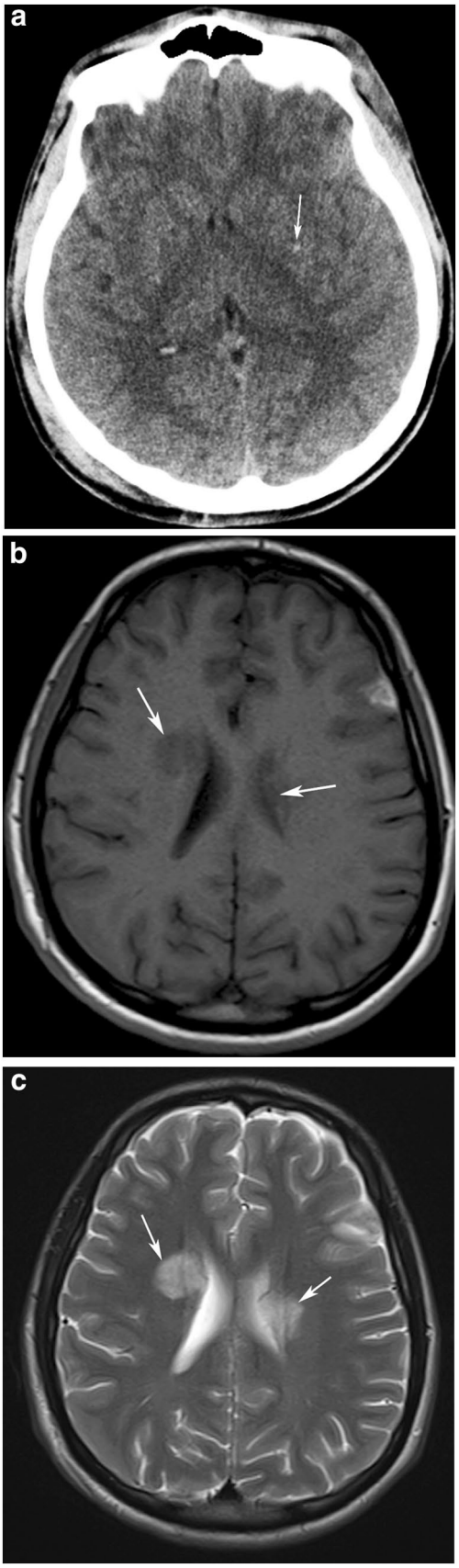

Fig. 12 A 15-year-old boy was presented after a motorcycle accident. **a** On axial NECT scan, hemorrhagic DAI is seen as increased density in the left basal ganglion (arrow). **b** On axial T1-W image, nonhemorrhagic DAI areas are seen as hypointense (arrows). **c** On axial T2-weighted image, they are seen as hyperintense areas in bilateral periventricular white matter (arrows). They were not seen in CT scan (not shown)

Cerebral contusion

High-energy trauma can cause blunt injury to the cortical gray matter which results in petechial hemorrhages with surrounding edema, defined as a contusion. Their characteristic locations are anterior frontal lobe and temporal lobe [47]. Cerebral contusions are described as "*coup*" and "*contrecoup*" lesions. Coup lesions occur at the site of impact, whereas contrecoup lesions are seen at the opposite site [45]. CT may be normal in the early phase of the blunt trauma. However, within time patchy, ill-defined lesions may arise as hyperdense foci with surrounding hypodense edema (Fig. 13).

MRI is more sensitive to detect cerebral contusions [48]. The age of hemorrhagic contusion is often recognized by its SI on T1- and T2-weighted images. On the other hand, the T2*-GRE sequence is the best imaging technique for the detection of hemorrhagic lesions (Fig. 14) [49]. Clinicians and radiologists should be on the alert for the coalescence of petechial hemorrhages which may result in hematomas and cerebral herniation. Therefore, the clinical worsening should be assessed as a premonitory symptom, especially in children, because they may show a rapid decline.

Traumatic vascular lesions

Traumatic cerebrovascular injuries include minimal intimal injury, dissection with intramural hematoma, pseudoaneurysm, occlusion, transection with active hemorrhage, and arteriovenous fistula. The most common mechanism of internal carotid artery (ICA) injury is hyperextension and contralateral rotation of the head. As a result, ICA gets stretched over the nearby transverse processes of C1 and C2 [18].

Traumatic dissection of the ICA involves the tearing of the tunica media, which causes bleeding into the arterial wall. The resultant thrombosis and vascular wall tearing are leading contributors of the pediatric stroke [50]. In clinical assessment, pain is an unexpected finding in children, but may be seen in adults. In imaging; MRI, CTA, MRA, and catheter angiography can be used for diagnosis. On T1-weighted imaging in MRI, an absence of signal void appearance or increased SI of ICA should be evaluated as a sign of dissection. The intimal flap can be seen in CTA or MRA. Narrowing of the vessel lumen on catheter angiography images is described as a "string sign," which leads to the

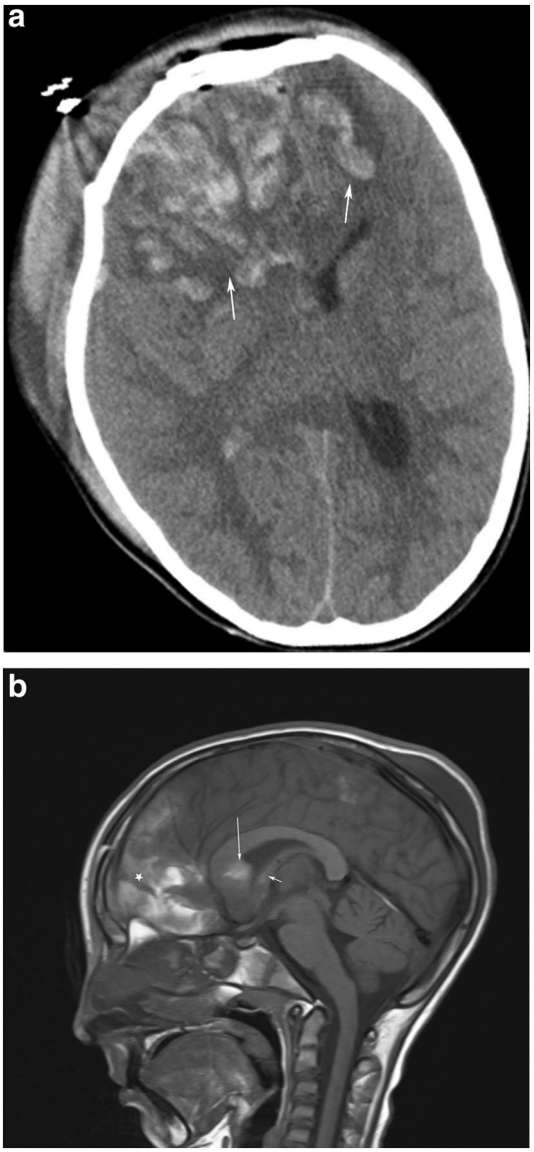

Fig. 13 A 12-year-old girl was presented after a road traffic accident. **a** Axial CT scan shows contusion areas in bilateral frontal lobes (arrows). Right lateral ventricle was compressed due to edema. **b** On sagittal T1-weighted image, contusion areas are seen as hyperintense areas in frontal lobe (star). High signal intensity of genu of the corpus callosum (long arrow) and fornix (short arrow) indicates hemorrhagic DAI

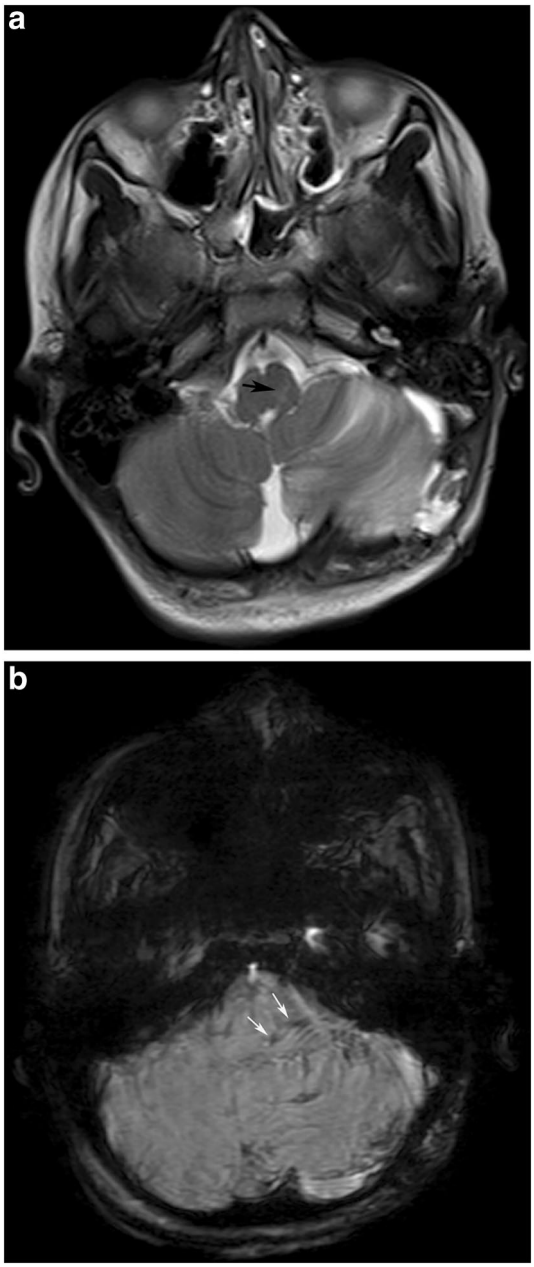

Fig. 14 A 9-year-old boy was presented with dysphagia after falling from 3 m while he riding a bike. **a** Axial T2-weighted image shows subtle high signal intensity in the left side of medulla oblangata (black arrow). **b** On SWI, microbleeding focus shows low signal intensity in the left side of medulla oblangata (white arrows)

diagnosis dissection (Fig. 15) [51]. In addition, the presence of a fractured carotid canal should increase the suspicion of dissection [52]. Pseudoaneurysm, another type of traumatic vascular lesion, is characterized by bubble formation from the native arterial wall which may become symptomatic 2–8 weeks after the trauma. On Doppler ultrasound, "*to and fro*" patterns and a "*yin–yang sign*" may appear due to forward and backward flow in pseudoaneurysms. Transection is the laceration of all three layers of the vessel wall also known as arterial rupture. Extravasation of contrast agent is an important finding of transection. Traumatic arteriovenous fistula (AVF) is rare and usually presents after the penetrating injury. AVF is an abnormal communication between an artery and vein. Carotid-cavernous fistula (CCF) is relatively more common than other traumatic AVF, in which a connection forms between the cavernous ICA and the cavernous sinus. On MRA, CTA or catheter angiography, dilatation of the ipsilateral superior ophthalmic vein and early

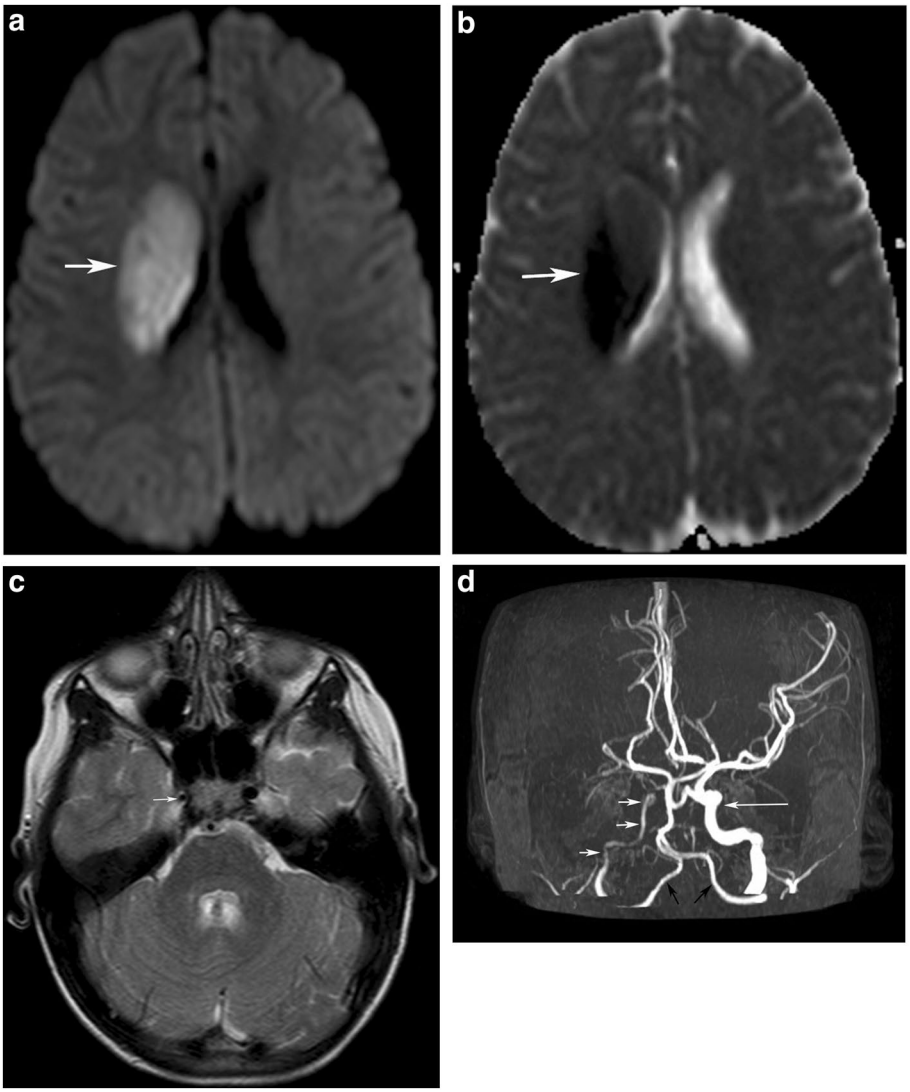

Fig. 15 A 6-year-old girl was presented with left hemiplegia after falling from a bicycle. **a** *b1000* DWI shows acute infarction with increased signal intensity in the right-sided basal ganglia. **b** It is seen as a hypointense area on the apparent diffusion coefficient map. **c** Axial T2-weighted image shows luminal narrowing of right ICA (arrow). **d** On coronal time-of-flight MR angiography maximum intensity projection image, string sign with luminal narrowing indicates the ICA dissection (short white arrows). Long arrow indicates left ICA and black arrows indicate bilateral vertebral arteries

enhancement of the cavernous sinus typically indicate CCF [53].

Diffuse cerebral edema

Cerebral swelling can be defined as the effacement of sulci, and compression of cisterns and ventricles. The underlying cause is either cerebral hyperemia or cerebral edema. Cerebral hyperemia represents increased blood volume due to dysautoregulation. The gray and white matter differentiation is preserved relatively in those patients [54]. Cerebral edema, characterized by loss of gray and white matter differentiation, can be divided into two categories: cytotoxic and vasogenic edema. The pathophysiology of the cerebral edema depends on the function of ATP-dependent Na/K pumps which may fail due to traumatic effects. Cytotoxic edema is characterized by an increase in water content within the intracellular compartment, which occurs in response to an osmotic gradient. On the other hand, vasogenic edema occurs as a result of blood–brain barrier disruption. Water moves from the vasculature to the extracellular space subsequently in response to an osmotic gradient [55].

Diffuse cerebral edema is an important entity, as it can result in ischemia and herniation. Aldrich EF et al. reported that diffuse cerebral edema is seen more commonly in children with head trauma than adults [56]. Imaging findings of diffuse cerebral edema on CT are as follows; diffuse cerebral parenchymal hypoattenuation and loss of normal differentiation of gray and white matter, effacement of sulci and cisterns, and compression of the ventricular system [57]. Children normally have small ventricular systems and a quite apparent perimesencephalic cistern; thus, compression or obliteration of those sites is readily recognized [58]. In diffuse cerebral edema, the cerebellum is relatively spared and appears hyperdense when compared with the cerebral parenchyma. This appearance is called "*reversal sign*" or

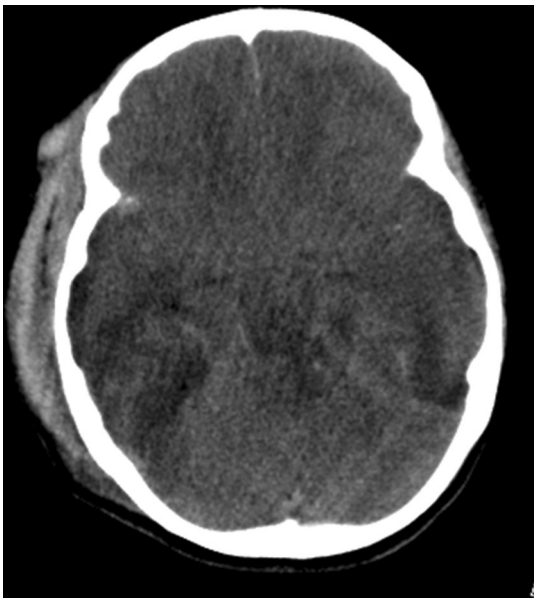

Fig. 16 A 12-year-old girl was presented after a road traffic accident with a diffuse cerebral edema. Axial NECT scan shows decreased attenuation of the brain parenchyma and relatively hyperdense cerebellum compared with the brain parenchyma which is called "*white cerebellum sign*"

"*white cerebellum sign*" (Fig. 16) [59, 60]. The other sign, "*Pseudosubarachnoid hemorrhage*," is an appearance of relatively hyperdense dura and tentorium in comparison with cerebral parenchyma (Fig. 17) [61]. This sign occurs due to the elevation of intracranial pressure which subsequently leads to narrowed subarachnoid space and engorgement and dilatation of pial vessels [13].

Traumatic hypoxic–ischemic brain injury (HIBI)

HIBI occurs when the mean arterial pressure falls below the lower limit of cerebral autoregulation. Thrombosis in the cerebral microcirculation is one of the causes of HIBI that may occur as a result of trauma. Intravascular thrombosis is more common in infants compared with older children and adults because of low flow states, hemoconcentration, and immature native antithrombotic pathways [62].

Patterns of HIBI vary highly according to brain maturation, and the severity and length of the insult [63, 64]. The most vulnerable areas to ischemic injury are vascular end zones (leading to so called "watershed infarctions"), the hippocampus, insular cortex, and basal ganglia [63, 64]. Acute hypoxic abnormalities are difficult to detect on T1- and T2-weighted sequences of MRI due to the brain's water content and incomplete myelination in children younger than 2 years of age [63]. DWI is superior to conventional MRI in traumatic HIBI diagnosis during the early phase of cerebral hypoxia [64]. The affected areas frequently demonstrate

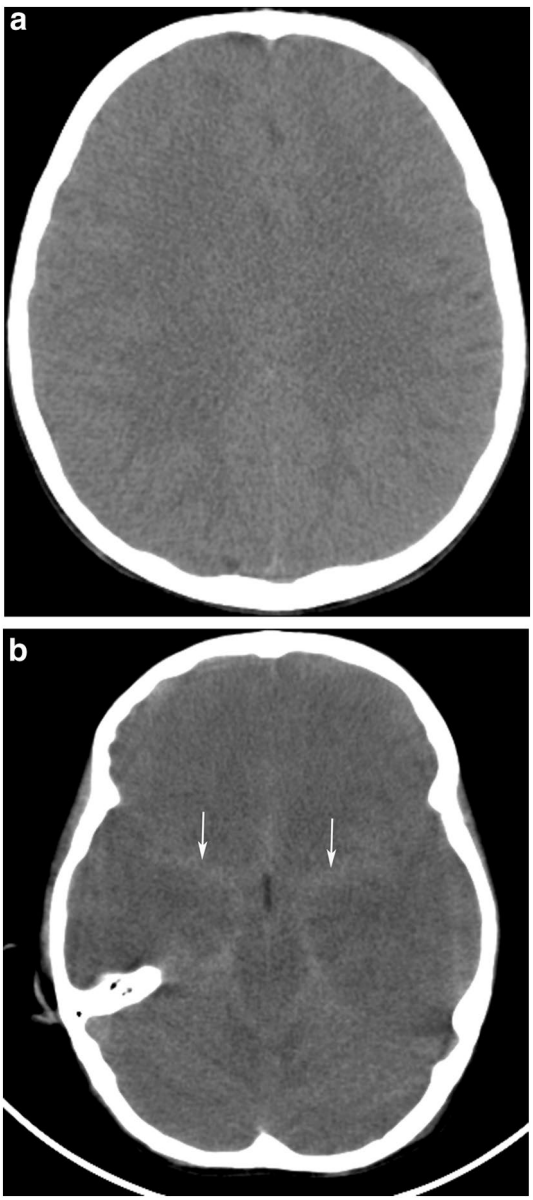

Fig. 17 A 7-year-old boy, who was found during the suicide attempt of hanging, had a diffuse cerebral edema. **a** Axial NECT scan, parenchymal low attenuation, effacement of sulci, and loss of differentiation gray and white matter indicate diffuse cerebral edema. **b** On axial NECT scan, pseudosubarachnoid hemorrhage is seen as effacement of basal cisterns and increased attenuation within them (arrows)

restricted diffusion (Fig. 18). In traumatic HIBI, CT scan might be normal. On the other hand, loss of normal differentiation of gray and white matters, hypodensity in deep gray matter, and "*white cerebellum*" sign may indicate HIBI associated with diffuse cerebral edema [65].

Another pattern of HIBI is the cortical laminar necrosis, which seems as a hyperintense cortical lesion on T1-weighted imaging in the subacute or chronic phase of

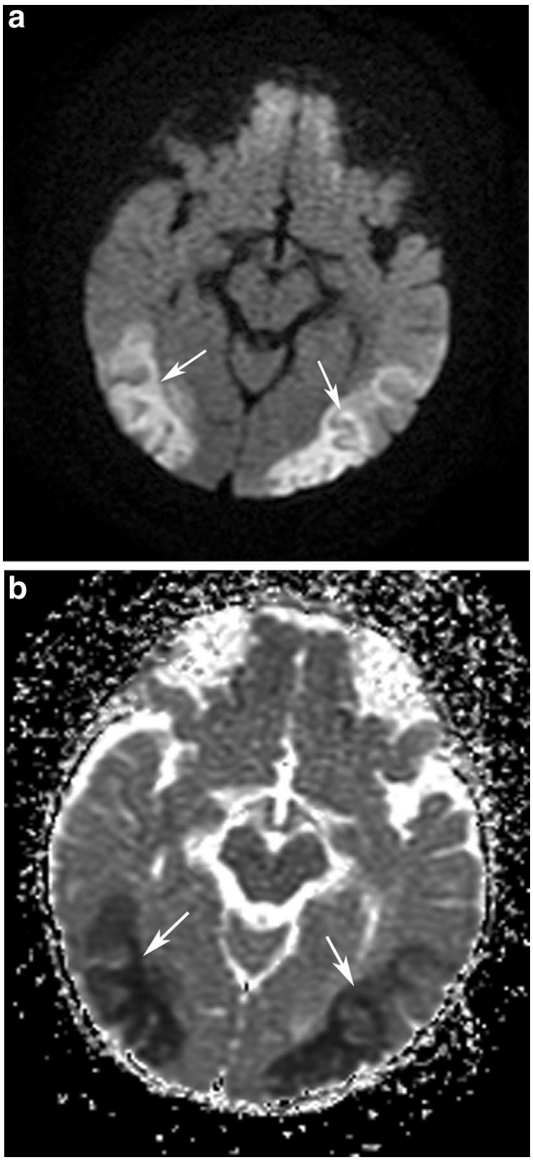

Fig. 18 A 4-month-old boy who was presented after falling from 2 m. *b1000* DWI image (**a**) and apparent diffusion coefficient map (**b**) show restricted diffusion in bilateral posterior border zone areas due to hypoxic–ischemic brain injury (arrows)

brain damage (Fig. 19). Cortical laminar necrosis occurs as a result of accumulation of denaturated proteins in dying cells after hypoxia [66, 67]. Similar to adults, most areas of cortical laminar necrosis in pediatric patients are nonhemorrhagic in imaging. Hemorrhage in cortical laminar necrosis after HIBI occurs rarely. On the other hand, Niwa et al. reported that small foci of hemorrhage in laminar necrotic areas detected by SWI might also be seen in meningoencephalitis, subacute infarction, and shaken baby syndrome [68].

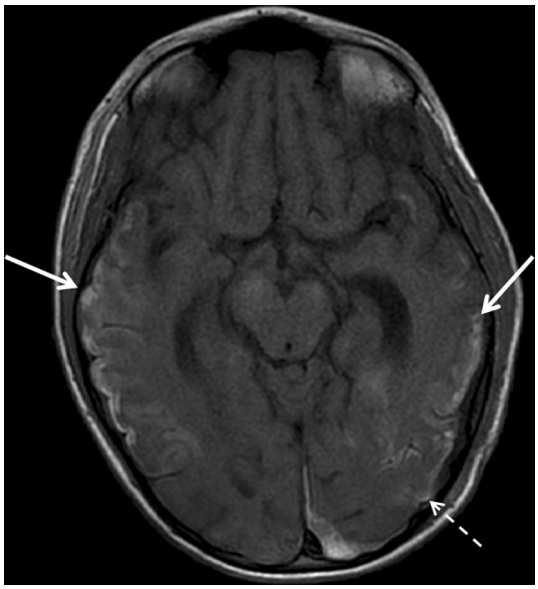

Fig. 19 A 9-year-old boy was presented after a road traffic accident. On axial T1-W image shows bilateral temporal (arrows) and left parietal (dashed arrow) cortical high signal intensity regarding cortical laminar necrosis from 3 to 5 days after trauma

Herniation

Increasing of brain volume depends on hemorrhage or edema which is initially compensated by displacement of CSF or blood. When the mechanism is overpassed, brain herniation may occur. Herniation may be divided into six main types (Fig. 20) [69]. Uncal herniation is the herniation of the medial temporal lobe downward from the tentorial incisura. It may be the cause of small linear hemorrhages along the midline of the brainstem (*Duret hemorrhages*). This herniation also causes compression of the ipsilateral

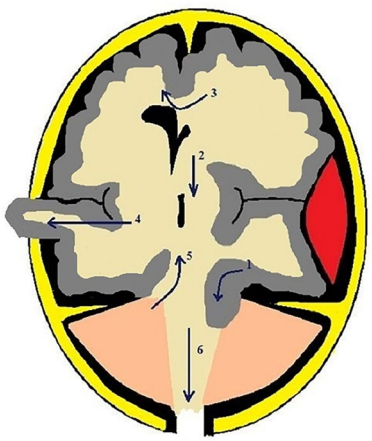

Fig. 20 Six types of brain herniation: (1) uncal, (2) central transtentorial, (3) subfalcine, (4) extracranial, (5) upward, and (6) tonsillar

third cranial nerve and posterior cerebral artery (PCA) and resulting in ipsilateral PCA territory infarction (Fig. 21) [70]. Another phenomenon associated with uncal herniation is the Kernohan's notch phenomenon. It occurs as a result of the compression of the cerebral peduncle against the tentorium cerebelli due to transtentorial herniation, and eventually, ipsilateral hemiparesis or hemiplegia may occur. This phenomenon is also named "*false localizing sign*" [71]. Central transtentorial herniation is herniation of the brainstem downward through the incisura, which may cause PCA infarction. Subfalcine herniation is herniation of the cingulate gyrus beneath the falx cerebri. Extracranial herniation is herniation of the brain tissue from a traumatic or iatrogenic calvarial defect (Fig. 22). Upward herniation is an upward movement of the cerebellum through the tentorium into the cranium. When either a large mass or increased pressure in the posterior fossa is present, the cerebellum is displaced in an upward direction through the tentorial opening. This herniation may also cause hydrocephalus due to upper brainstem compression and aqueductal stenosis. Finally, tonsillar herniation is the herniation of cerebellar tonsils downward below the foramen magnum. Following tonsillar herniation, compression of the lower brainstem and medullary respiratory centers may cause sudden death.

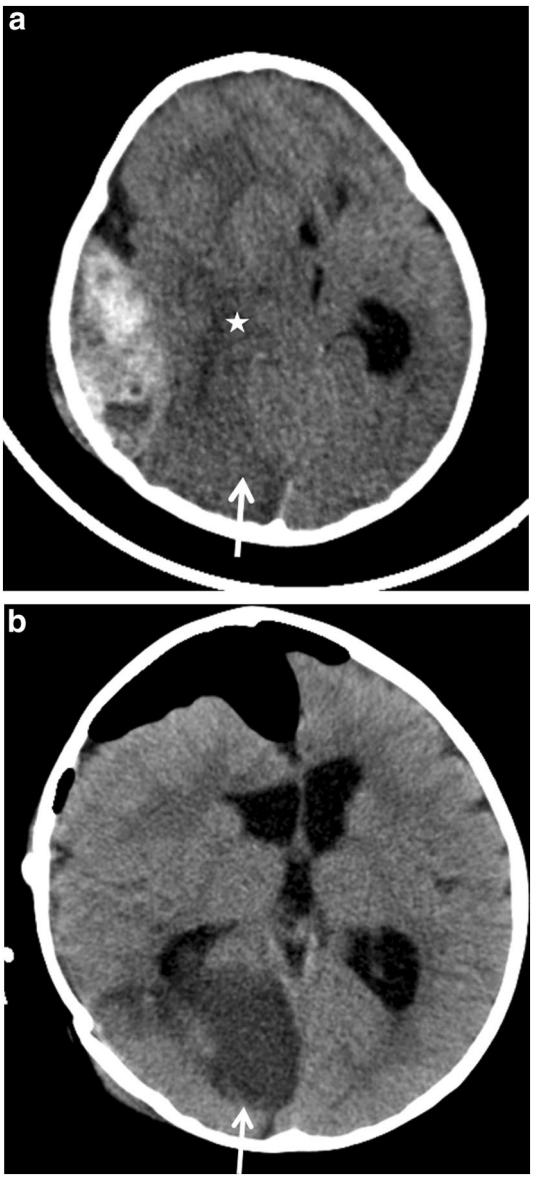

Fig. 21 A 1-year-old girl was presented after falling from 5 m. **a** Preoperative axial NECT scan shows epidural hematoma, uncal herniation of right medial temporal lobe (star), and loss of normal differentiation of gray and white matters in occipital lobe (arrow). **b** Postoperative axial NECT scan shows right occipital lobe infarction due to the compression of ipsilateral posterior cerebral artery

Cerebral spinal fluid leakage

CSF leakage is the movement of CSF from the intracranial cavity through an osseous defect in the skull base [72]. Most common location of the traumatic CSF leakage is the anterior cranial fossa. Fractures of the frontal sinus wall, cribriform plate or temporal bone may result in CSF leakage. Clinical findings usually develop in the first 48 h after injury. A small subset of patients presents with rhinorrhea or meningitis several years after the trauma.

CT findings that increase the suspicion of CSF leakage are pneumocephalus and the air–fluid level in paranasal sinuses (Fig. 23). In addition, an asymmetrical opacification in mastoid cells and middle ear cavity, fracture of the tegmen tympani or inner ear structure may indicate the CSF leakage [72]. Diagnosing the defective area may be difficult in routine CT scans, so that MR cisternography may be used as an adjunct to CT. Undiagnosed CSF leakage may

Fig. 22 On axial NECT scan, extracranial herniation of right frontoparietal lobe is seen after decompression craniectomy (the same case in Fig. 13)

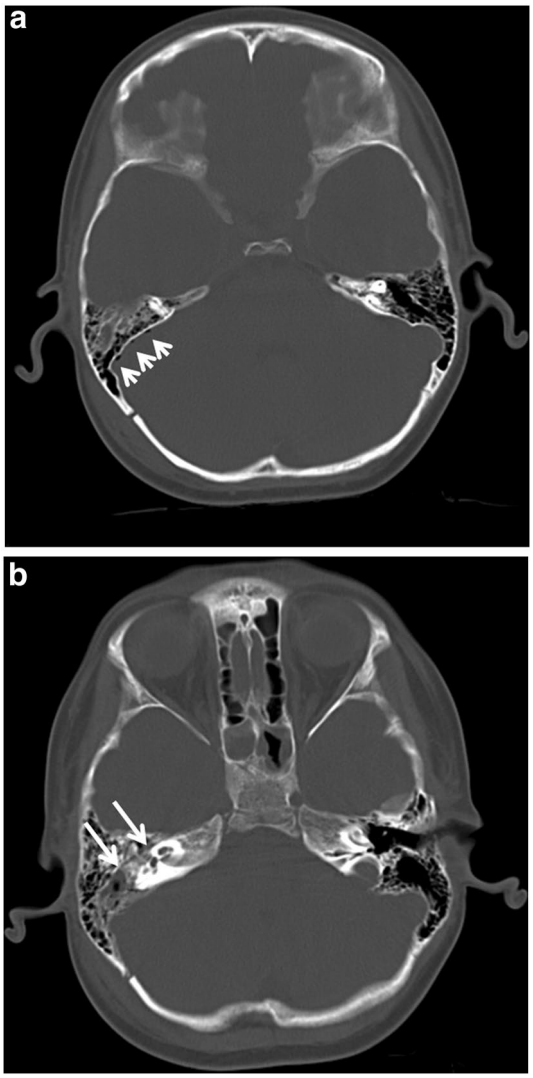

Fig. 23 A 10-year-old boy was presented after a road traffic accident. He had otorrhea in the right side on physical examination. Axial NECT scan (**a, b**) shows pneumocephalus (short arrows) and temporal bone fracture (long arrows). Note that hemorrhagic opacification is seen in right mastoid cells

get complicated with the development of meningitis or an intracranial abscess.

Encephalomalacia and atrophy

Encephalomalacia consists of the softening or loss of brain tissue with surrounding gliosis and dilatation of the adjacent ventricle. The term is usually used to describe blurred cortical margins and decreased consistency of brain tissue. It occurs in the late period after the trauma. The appearance of encephalomalacia is not specific for post-traumatic injury, but the locations are characteristic: antero-inferior frontal and temporal lobes [73]. Encephalomalacia shows the same signal intensity with CSF on MR sequences, whereas gliotic

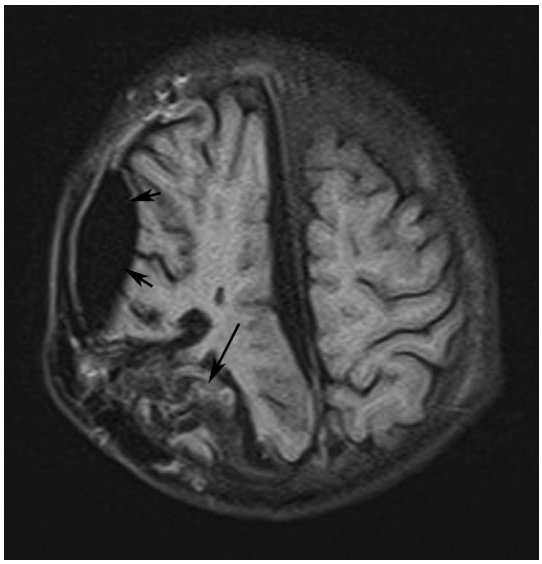

Fig. 24 Axial FLAIR image shows encephalomalacia which has a higher signal intensity than CSF in right parietal lobe (long black arrow). In addition, a pseudomeningocele is seen which is signed with short black arrows (the same case in Fig. 5)

brain tissue shows high signal intensity on T2-weighted and FLAIR images (Fig. 24) [73]. Diffuse parenchymal atrophy and tissue loss may occur in the late phase of brain swelling, increased intracranial pressure, and hypoxia in traumatic patients.

Severe head injury may also cause atrophy of the corpus callosum which indicates the disruption of interhemispheric connections regarding the chronicity of the injury. In addition, loss of forniceal and hippocampal volume may occur in association with trauma.

White matter changes related to TBI can be demonstrated with DTI. DTI has several quantifiable parameters [e.g., fractional anisotropy (FA), axial diffusivity, radial diffusivity, and mean diffusivity] [20, 74]. FA yields the primary measure of white matter integrity, with values ranging from 0 to 1. Values close to 0 indicate diffusion impairment in an injured white matter, whereas values close to 1 correspond to normal (or anisotropic) diffusivity in the healthy white matter [75]. Although several studies have reported that FA values increase in both acute and chronic TBI [76, 77], most studies of TBI have suggested that decreases in FA and increases in mean diffusivity correspond to demyelination or disruption of white matter integrity [78, 79].

Non-accidental head trauma (NAT)

NAT is the leading cause of morbidity and mortality in infants and children. NAT is characterized by a combination of intracranial injuries, retinal hemorrhages, and bone fractures [80]. It is more common in children aged < 2 years,

since the majority of those injuries occurs during the first year of life [81]. Because infants have weaker neck muscles, a larger head compared with the body, and a wider subarachnoid space than children and adults, they are more prone to NAT.

The initial imaging procedure used is commonly CT; however, MRI should be performed in NAT cases, irrespective of negative findings on head CT scans. SDH, diffuse cerebral edema, HIBI, and DAI are common findings in NAT [57]. The prevalence of skull fractures in all cases of child abuse is approximately 8–13% [82]. Studies have shown that multiple fractures, fractures that cross sutures, and bilateral fractures are more likely to be associated with the child abuse [83–85].

SDH and SAH, which are usually caused by high-energy angular or rotational acceleration/ deceleration forces delivered during shaking or shaking impact assaults, are more common in NAT. Shear strain forces result in disruption of delicate cortical bridging veins. In contrast, EDH is particularly uncommon in cases of abuse [83, 86]. Especially, different ages of subdural hematomas should raise the suspicion of NAT. In patients with NAT, SDH is often located in the interhemispheric fissure or infratentorially with/without accompanying intraparenchymal hemorrhage [87].

The three most common patterns of brain parenchymal injury in NAT are DAI, cerebral edema, and contusion. Focal or diffuse edema is more common than other parenchymal injuries in NAT [57]. Although any head injury, including scalp contusion, skull fracture, epidural hematoma, and cerebral contusion, can be demonstrated in cases of abuse, clinicians and radiologists should bear in mind the possibility of SDH.

Finally, the radiologic findings must be interpreted in the context of clinical history and results of the physical examination.

Conclusion

In this article, we provide a comprehensive review for pediatric TBI with an emphasis on imaging findings as well as the current algorithms to guide the clinicians about the appropriate time of CT scanning. Children are not just "little adults," and response to the head trauma have many differences in children when compared with adults; therefore, trauma algorithms also differ. In the literature, PECARN, CHALICE, and CATCH algorithms are described for children with head trauma in order to decide the necessity of a CT scan. In all of the algorithms, the decision is based on history, clinical examination, and the mechanism of trauma. Although it is not possible to directly compare them, some studies have shown that PECARN rule is more sensitive than the others which includes much more specific patient population.

Early and late phase lesions, such as skull fractures, hemorrhages, parenchymal lesions, vascular lesions, caused by head trauma, are reliably recognized by CT scanning and MRI. Some hemorrhagic lesions and HIBI may be overlooked when using only CT and conventional MRI sequences. Due to the possibility of a normal CT scan, MR imaging including DWI and T2*-GRE sequences should be performed in selected cases with higher risk, such as patients with GCSS < 15 at 2 h after injury, in cases of open or depressed skull fracture suspicion, history of worsening headache, irritability, or worsening symptoms. Undiagnosed traumatic brain lesions may cause permanent and serious damages. Children who have suffered a head trauma should be closely followed-up clinically and radiologically for delayed complications of trauma.

Compliance with ethical standards

Conflict of interest Fatma Ceren Sarioglu, Hilal Sahin, Yeliz Pekcevik, Orkun Sarioglu, and Ozgur Oztekin declare that they have no conflict of interest.

Informed consent This is a retrospective article; therefore, informed consent was not applicable.

Research involving human and animal participants This article does not contain any studies with human participants or animals performed by any of the authors.

References

1. Sarioglu FC, Sahin H, Pekcevik Y, Sarioglu O, Oztekin O. Pediatric head trauma: common and uncommon imaging findings. ECR C-1022. 2016. doi:10.1594/ecr2016/C-1022.
2. Giza CC. Lasting effects of pediatric traumatic brain injury. IJNT. 2006;3(1):19–26.
3. Alexiou GA, Sfakianos G, Prodromou N. Pediatric head trauma. J Emerg Trauma Shock. 2011;4(3):403–8.
4. Kuppermann N, Holmes JF, Dayan PS, Hoyle JD Jr, Atabaki SM, Holubkov R, et al. Identification of children at very low risk of clinically-important brain injuries after head trauma: a prospective cohort study. Lancet. 2009;374(9696):1160–70.
5. Dunning J, Daly JP, Lomas JP, Lecky F, Batchelor J, Mackway-Jones K, et al. Derivation of the children's head injury algorithm for the prediction of important clinical events decision rule for head injury in children. Arch Dis Child. 2006;91(11):885 – 91.
6. Osmond MH, Klassen TP, Wells GA, Correll R, Jarvis A, Joubert G, et al. CATCH: a clinical decision rule for the use of computed tomography in children with minor head injury CMAJ. 2010;182(4):341–8.
7. Babl FE, Borland ML, Phillips N, Kochar A, Dalton S, McCaskill M, et al. Accuracy of PECARN, CATCH, and CHALICE head injury decision rules in children: a prospective cohort study. Lancet. 2017. doi:10.1016/S0140-6736(17)30555-X. (Epub ahead of print).

8. Easter JS, Bakes K, Dhaliwal J, Miller M, Caruso E, Haukoos JS. Comparison of PECARN, CATCH, and CHALICE rules for children with minor head injury: a prospective cohort study. Ann Emerg Med. 2014;64(2):145 – 52.
9. Davis PC. Head trauma. AJNR Am J Neuroradiol. 2007;28(8):1619–21.
10. Pearce MS, Salotti JA, Little MP, McHugh K, Lee C, Kim KP, et al. Radiation exposure from CT scans in childhood and subsequent risk of leukaemia and brain tumours: a retrospective cohort study. Lancet. 2012;380(9840):499–505.
11. Iliescu IA. Current diagnosis and treatment of chronic subdural haematomas. J Med Life. 2015;8(3):278 – 84.
12. Senturk S, Guzel A, Bilici A, Takmaz I, Guzel E, Aluclu MU, et al. CT and MR imaging of chronic subdural hematomas: a comparative study. Swiss Med Wkly. 2010;140:(23–4):335–40.
13. Provenzale J. CT and MR imaging of acute cranial trauma. Emerg Radiol. 2007;14(1):1–12.
14. Haacke EM, Mittal S, Wu Z, Neelavalli J, Cheng YC. Susceptibility-weighted imaging: technical aspects and clinical applications, part 1. AJNR Am J Neuroradiol. 2009;30(1):19–30.
15. Mittal S, Wu Z, Neelavalli J, Haacke EM. Susceptibility-weighted imaging: technical aspects and clinical applications, part 2. AJNR Am J Neuroradiol. 2009;30(2):232 – 52.
16. Wu Z, Mittal S, Kish K, Yu Y, Hu J, Haacke EM. Identification of calcification with magnetic resonance imaging using susceptibility-weighted imaging: a case study. J Magn Reson Imaging. 2009;29(1):177–82.
17. Kohler R, Vargas MI, Masterson K, Lovblad KO, Pereira VM, Becker M. CT and MR angiography features of traumatic vascular injuries of the neck. AJR Am J Roentgenol. 2011;196(6):800–9.
18. Sliker CW. Blunt cerebrovascular injuries: imaging with multidetector CT angiography. Radiographics. 2008;28(6):1689 – 708.
19. Biffl WL, Moore EE, Offner PJ, Burch JM. Blunt carotid and vertebral arterial injuries. World J Surg. 2001;25(8):1036–43.
20. Wintermark M, Sanelli PC, Anzai Y, Tsiouris AJ, Whitlow CT. Imaging evidence and recommendations for traumatic brain injury: advanced neuro and neurovascular imaging techniques. AJNR Am J Neuroradiol. 2015;36(2):1–11.
21. Shenton ME, Hamoda HM, Schneiderman JS, Bouix S, Pasternak O, Rathi Y, et al. A review of magnetic resonance imaging and diffusion tensor imaging findings in mild traumatic brain injury. Brain Imaging Behav. 2012;6(2):137 – 92.
22. Forster BB, MacKay AL, Whittall KP, Kiehl KA, Smith AM, Hare RD, et al. Functional magnetic resonance imaging: the basics of blood-oxygen-level dependent (BOLD) imaging. Can Assoc Radiol J. 1998;49(5):320–9.
23. Mayer AR, Bellgowan PS, Hanlon FM. Functional magnetic resonance imaging of mild traumatic brain injury. Neurosci Biobehav Rev. 2015;49:8–18.
24. Cohen BA, Inglese M, Rusinek H, Babb JS, Grossman RI, Gonen O. Proton MR spectroscopy and MRI-volumetry in mild traumatic brain injury. AJNR Am J Neuroradiol. 2007;28(5):907 – 13.
25. Vagnozzi R, Signoretti S, Cristofori L, Alessandrini F, Floris R, Isgrò E, et al. Assessment of metabolic brain damage and recovery following mild traumatic brain injury: a multicentre, proton magnetic resonance spectroscopic study in concussed patients. Brain. 2010;133(11):3232–42.
26. Udomphorn Y, Armstead WM, Vavilala MS. Cerebral blood flow and autoregulation after pediatric traumatic brain injury. Pediatr Neurol. 2008;38(4):225 – 34.
27. Idriz S, Patel JH, Ameli Renani S, Allan R, Vlahos I. CT of normal developmental and variant anatomy of the pediatric skull: distinguishing trauma from normality. Radiographics. 2015;35(5):1585 – 601.
28. Khandelwal S, Sharma GL, Gopal S, Sakhi P. Growing skull fractures/leptomeningeal cyst. Indian J Radiol Imaging. 2002;12(4):485–6.
29. Glass RB, Fernbach SK, Norton KI, Choi PS, Naidich TP. The infant skull: a vault of information. Radiographics. 2004;24(2):507 – 22.
30. Hollon T, McKeever PE, Garton HJ, Maher CO. Skull fracture mimicking eosinophilic granuloma. Childs Nerv Syst. 2015;31(7):1171–4.
31. Zayas JO, Feliciano YZ, Hadley CR, Gomez AA, Vidal JA. Temporal bone trauma and the role of multidetector CT in the emergency department. Radiographics. 2011;31(6):1741–55.
32. Turel KE, Sharma NK, Verghese J, Desai S. Post traumatic facial paralysis treatment options and strategies. IJNT. 2005;2(1):33 – 4.
33. Pekçevik Y, Hasbay E, Pekçevik R. Three-dimensional CT imaging in pediatric calvarial pathologies. Diagn Interv Radiol. 2013;19(6):488 – 94.
34. Orman G, Wagner MW, Seeburg D, Zamora CA, Oshmyansky A, Tekes A, et al. Pediatric skull fracture diagnosis: should 3D CT reconstructions be added as routine imaging? J Neurosurg Pediatr. 2015;16(4):426 – 31.
35. Singh S, Ramakrishnaiah RH, Hegde SV, Glasier CM. Compression of the posterior fossa venous sinuses by epidural hemorrhage simulating venous sinus thrombosis: CT and MR findings. Pediatr Radiol. 2016;46(1):67–72.
36. Bullock MR, Chesnut R, Ghajar J, Gordon D, Hartl R, Newell DW, et al. Surgical management of acute epidural hematomas Neurosurgery. 2006;58(3 suppl):S7–15.
37. Dalgiç A, Seçer M, Ergüngör F, Okay O, Akdağ R, Ciliz D. Dural sinus thrombosis following head injury: report of two cases and review of the literature. Turk Neurosurg. 2008;18(1):70 – 7.
38. Momose H, Sorimachi T, Aoki R, Atsumi H, Matsumae M. Cerebral infarction following acute subdural hematoma in infants and young children: predictors and significance of FLAIR vessel hyperintensity. Neurol Med Chir (Tokyo). 2015;55(6):510–8.
39. Sieswerda-Hoogendoorn T, Postema FA, Verbaan D, Majoie CB, van Rijn RR. Age determination of subdural hematomas with CT and MRI: a systematic review. Eur J Radiol. 2014;83(7):1257–68.
40. Stuckey SL, Goh TD, Heffernan T, Rowan D. Hyperintensity in the subarachnoid space on FLAIR MRI. AJR Am J Roentgenol. 2007;189(4):913 – 21.
41. Woodcock RJ Jr, Short J, Do HM, Jensen ME, Kallmes DF. Imaging of acute subarachnoid hemorrhage with a fluid-attenuated inversion recovery sequence in an animalmodel: comparison with non-contrast-enhanced CT. AJNR Am J Neuroradiol. 2001;22(9):1698–703.
42. Wu Z, Li S, Lei J, An D, Haacke EM. Evaluation of traumatic subarachnoid hemorrhage using susceptibility-weighted imaging. AJNR Am J Neuroradiol. 2010;31(7):1302–10.
43. Liu AY, Maldjian JA, Bagley LJ, Sinson GP, Grossman RI. Traumatic brain injury: diffusion-weighted MR imaging findings. AJNR Am J Neuroradiol. 1999;20(9):1636–41.
44. Adams JH, Doyle D, Ford I, Gennarelli TA, Graham DI, McLellan DR. Diffuse axonal injury in head injury: definition, diagnosis and grading. Histopathology. 1989;15(1):49–59.
45. Kim JJ, Gean AD. Imaging for the diagnosis and management of traumatic brain injury. Neurother. 2011;8(1):39–53.
46. Schaefer PW, Huisman TA, Sorensen AG, Gonzalez RG, Schwamm LH. Diffusion-Weighted MR imaging in closed head injury: high correlation with initial glasgow coma scale score and score on modified Rankin scale at discharge. Radiology. 2004;233(1):58–66.
47. Currie S, Saleem N, Straiton JA, Macmullen-Price J, Warren DJ, Craven IJ. Imaging assessment of traumatic brain injury. Postgrad Med J. 2016;92(1083):41–50.

48. Morais DF, Spotti AR, Tognola WA, Gaia FF, Andrade AF. Clinical application of magnetic resonance in acute traumatic brain injury. Arq Neuropsiquiatr. 2008;66(1):53 – 8.
49. Suskauer SJ, Huisman TA. Neuroimaging in pediatric traumatic brain injury: current and future predictors of functional outcome. Dev Disabil Res Rev. 2009;15(2):117–23.
50. Mortazavi MM, Verma K, Tubbs RS, Harrigan M. Pediatric traumatic carotid, vertebral and cerebral artery dissections: a review. Childs Nerv Syst. 2011;27(12):2045–56.
51. Pappas JN. The Angiographic String Sign. Radiology. 2001;222:237–8.
52. York G, Barboriak D, Petrella J, DeLong D, Provenzale JM. Association of internal carotid artery injury with carotid canal fractures in patients with head trauma. AJR Am J Roentgenol. 2005;184(5):1672–8.
53. Chen CC, Chang PC, Shy CG, Chen WS, Hung HC. CT angiography and MRangiography in the evaluation of carotid cavernous sinus fistula prior to embolization: a comparison of techniques. AmJ Neuroradiol. 2005;26(9):2349–56.
54. Yoshino E, Yamaki T, Higuchi T, Horikawa Y, Hirakawa K. Acute brain edema in fatal head injury: analysis by dynamic CT scanning. J Neurosurg. 1985;63(6):830–9.
55. Donkin JJ, Vink R. Mechanisms of cerebral edema in traumatic brain injury: therapeutic developments. Curr Opin Neurol. 2010;23(3):293–9.
56. Aldrich EF, Eisenberg HM, Saydjari C, Luerssen TG, Foulkes MA, Jane JA, et al. Diffuse brain swelling in severely head-injured children. A report from the NIH Traumatic Coma Data Bank. J Neurosurg. 1992;76(3):450–4.
57. Lonergan GJ, Baker AM, Morey MK, Boos SC. From the archives of the AFIP. Child abuse: radiologic-pathologic correlation. Radiographics. 2003;23(4):811 – 45.
58. Zimmerman RA, Bilaniuk LT, Bruce D, Dolinskas C, Obrist W, Kuhl D. Computed tomography of pediatric head trauma: acute general cerebral swelling. Radiology. 1978;126(2):403–8.
59. Han BK, Towbin RB, De Courten-Myers G, McLaurin RL, Ball WS Jr. Reversal sign on CT: effect of anoxic/ischemic cerebral injury in children. AJR Am J Roentgenol. 1990;154(2):361–8.
60. Harwood-Nash. DC Abuse to the pediatric central nervous system. AJNR Am J Neuroradiol. 1992;13(2):569 – 75.
61. Given CA, Burdette JH, Elster AD, Williams DW. Pseudosubarachnoid hemorrhage: a potential imaging pitfall associated with diffuse cerebral edema. AJNR Am J Neuroradiol. 2003;24(2):254–6.
62. Ichord RN, Naim M, Pollock AN, Nance ML, Margulies SS, Christian CW. Hypoxic-ischemic injury complicates inflicted and accidental traumatic brain injury in young children: the role of diffusion-weighted imaging. J Neurotrauma. 2007;24(1):106 – 18.
63. Huang BY, Castillo M. Hypoxic-ischemic brain injury: imaging findings from birth to adulthood. Radiographics. 2008;28(2):417 – 39.
64. White ML, Zhang Y, Helvey JT, Omojola MF. Anatomical patterns and correlated MRI findings of non-perinatal hypoxic–ischaemic encephalopathy. Br J Radiol. 2013;86(1021):20120464.
65. Haque IU, Udassi JP, Zaritsky AL. Outcome following cardiopulmonary arrest. Pediatr Clin North Am. 2008;55(4):969–87.
66. Kesavadas C, Santhosh K, Thomas B, Gupta AK, Kapilamoorthy TR, Bodhey N, et al. Signal changes in cortical laminar necrosis: evidence from susceptibility-weighted magnetic resonance imaging. Neuroradiology. 2009;51(5):293–8.
67. Kinoshita T, Ogawa T, Yoshida Y, Tamura H, Kado H, Okudera T. Curvilinear T1 hyperintense lesions representing cortical necrosis after cerebral infarction. Neuroradiology. 2005;47(9):647 – 51.
68. Niwa T, Aida N, Shishikura A, Fujita K, Inoue T. Susceptibility-weighted imaging findings of cortical laminar necrosis in pediatric patients. AJNR Am J Neuroradiol. 2008;29(9):1795–8.
69. Head HW, Kandula VR, Shekdar KV, Polloc AV. Key imaging findings in acute cerebral herniation syndromes in pediatric patients. The children's hospital of Philadelphia 2009. http://www.pedrad.org/Portals/5/Events/2009/HeadHerniation.pdf.
70. Aiken AH, Gean AD. Imaging of head trauma. Semin Roentgenol. 2010;45(2):63–79.
71. McKenna C, Fellus J, Barrett AM. False localizing signs in traumatic brain injury. Brain Inj. 2009;23(7):597–601.
72. Lloyd KM, DelGaudio JM, Hudgins PA. Imaging of skull base cerebrospinal Fluid Leaks in Adults. Radiology. 2008;248(3):725 – 36.
73. Brant WE, Helms CA. Fundemantals of diagnostic radiology. 4th edn. Philedelphia: Lippincott Williams & Wilkins; 2012.
74. Kraus MF, Susmaras T, Caughlin BP, Walker CJ, Sweeney JA, Little DM. White matter integrity and cognition in chronic traumatic brain injury: a diffusion tensor imaging study. Brain. 2007;130:2508–19.
75. Le Bihan D, Mangin JF, Poupon C, Clark CA, Pappata S, Molko N, et al. Diffusion tensor imaging: concepts and applications. J Magn Reson Imaging. 2001;13(4):534 – 46.
76. Wilde EA, McCauley SR, Hunter JV, Bigler ED, Chu Z, Wang ZJ, et al. Diffusion tensor imaging of acute mild traumatic brain injury in adolescents. Neurology. 2008;70(12):948–55.
77. Bazarian JJ, Zhong J, Blyth B, Zhu T, Kavcic V, Peterson D. Diffusion tensor imaging detects clinically important axonal damage after mild traumatic brain injury: a pilotstudy. J Neurotrauma. 2007;24(9):1447–59.
78. Tisserand DJ, Stanisz G, Lobaugh N, Gibson E, Li T, Black SE, et al. Diffusion tensor imaging for the evaluation of white matter pathology in traumatic brain injury. Brain Cogn. 2006;60(2):216–7.
79. Xu J, Rasmussen IA, Lagopoulos J, Håberg A. Diffuse axonal injury in severe traumatic brain injury visualized using high-resolution diffusion tensor imaging. J Neurotrauma. 2007;24(5):753–65.
80. Caffey J. The whiplash shaken infant syndrome: manual shaking by the extremity with whiplash-induced intracranial and intraocular bleeding, linked with residual permanent brain damage and mental retardation. Pediatrics. 1974;54:396–403.
81. Dashti SR, Decker DD, Razzaq A, Cohen AR. Current patterns of inflicted head injury in children. Pediatr Neurosurg. 1999;31(6):302–6.
82. King J, Diefendorf D, Apthorp J, Negrete VF, Carlson M. Analysis of 429 fractures in 189 battered children. J Pediatr Orthop. 1988;8(5):585–9.
83. Meservy CJ, Towbin R, McLaurin RL, Myers PA, Ball W. Radiographic characteristics of skull fractures resulting from child abuse. AJR Am J Roentgenol. 1987;149(1):173–5.
84. Merten DF, Osborne DR, Radkowski MA, Leonidas JC. Craniocerebral trauma in the child abuse syndrome: radiological observations. Pediatr Radiol. 1984;14(5):272–7.
85. Hobbs CJ. Skull fracture and the diagnosis of abuse. Arch Dis Child. 1984;59(3):246–52.
86. Shugerman RP, Paez A, Grossman DC, Feldman KW, Grady MS. Epidural hemorrhage: is it abuse? Pediatrics. 1996;97(5):664–8.
87. Foerster BR, Petrou M, Lin D, Thurnher MM, Carlson MD, Strouse PJ, et al. Neuroimaging evaluation of non-accidental head trauma with correlation to clinical outcomes: a review of 57 cases. J Pediatr. 2009;154(4):573–7.